Available online at www.sciencedirect.com
SCIENCE DIRECT
Journal of Catalysis 232 (2005) 161–178
JOURNAL OF CATALYSIS
www.elsevier.com/locate/jcat

A density functional theory comparison of anatase (TiO_2)- and γ-Al_2O_3-supported MoS_2 catalysts

C. Arrouvel [a], M. Breysse [b], H. Toulhoat [c], P. Raybaud [a,*]

[a] *Direction Chimie et Physico-Chimie Appliquées, Institut Français du Pétrole, 1-4 avenue de Bois-Préau, 92852 Rueil-Malmaison cedex, France*
[b] *Laboratoire de Réactivité de Surface - UMR 7609 CNRS, Université Pierre et Marie Curie, 4 Place Jussieu, 75252 Paris cedex 05, France*
[c] *Direction Scientifique, Institut Français du Pétrole, 1-4 avenue de Bois-Préau, 92852 Rueil-Malmaison cedex, France*

Received 16 November 2004; revised 11 February 2005; accepted 16 February 2005

Available online 7 April 2005

Abstract

Using density functional theory periodic calculations, we investigate the effects of two relevant supports for industrial hydrodesulfurization catalysts, anatase (titania) and γ-alumina, on the thermodynamic stability of Mo_6S_n ($n = 10$ to 24) clusters representing the MoS_2 active phase. Under HDS conditions, anatase surfaces stabilize more sulfur-deficient small clusters than alumina surfaces. Because of an epitaxy relationship, the anatase surfaces also enhance tilted and perpendicular cluster orientations. For large cluster sizes, we establish a model extrapolating the energetic properties obtained on supported Mo_6S_n clusters that reveals how the nature of the chemical interaction of the MoS_2 single layer is modified. A concept based on competing "ligand effects" between the support and the gas phase on the active phase is proposed to explain our results. These new insights are in line with the higher intrinsic HDS activity reported for the anatase-supported MoS_2 catalyst.

Keywords: Anatase (TiO_2); γ-Al_2O_3; MoS_2; Hydrodesulfurization (HDS); Surface; Density functional theory (DFT); Ligand effects; Epitaxy

1. Introduction

Industrial hydrodesulfurization (HDS) catalysts are made of γ-alumina-supported Co(Ni)MoS. Numerous experimental insights have been obtained on the catalytic active phase [1,2]. At the same time, much progress has been achieved in the synthesis and preparation of the γ-alumina support [3] and titania [4] with the goal of improving ion exchange and textural properties. Characterization techniques such as EXAFS [5,6], TEM [7], infrared (IR) spectroscopy [8,9], and UV–vis diffuse reflectance spectroscopy (DRS) [10] have been successfully applied to γ-alumina- or anatase (titania)-supported catalysts but have now reached their limits in providing any more relevant insights at the interface between the active phase and the support. Furthermore, no clear interpretation of the support effect on HDS catalytic activities has emerged. Some of us have found that the turnover frequency in thiophene HDS is about 4.4 times higher for titania-supported than for γ-alumina-supported MoS_2 [11–13]. Electronic effects [11], orientation effects [7], and even direct promotion by Ti [10,14,15] have been invoked; however, no rational explanation has been provided so far. As a consequence, new insights are mandatory for making progress in this field.

Density functional theory (DFT)-based simulations have proved to be efficient for characterizing the active sites of MoS_2-based nanocatalysts [16–22] and for the surface properties of γ-alumina and anatase supports [23–27] under sulfo-reductive conditions. Some theoretical studies [28–30] have attempted to address the difficult question of the interaction of the MoS_2 active phase with the alumina support. However, they suffer from weaknesses, particularly in the representation of stable γ-alumina surface chemical species (including hydroxyl groups) under HDS conditions. The size

* Corresponding author. Fax: +33 1 47 52 70 58.
E-mail address: pascal.raybaud@ifp.fr (P. Raybaud).

0021-9517/$ – see front matter
doi:10.1016/j.jcat.2005.02.018

of the $Al_2O_5H_2$ cluster used in [28] is too modest to permit a correct description of the electronic features of the support. The representation of the support by Ionescu et al. [29] with spinel-like ideal surfaces without consideration of their hydroxylation states is inappropriate. Even if numerous theoretical studies still focus on the spinel-based model, recent extensive DFT works [23–25] have also shown that this ideal model is not suitable for γ-alumina as produced industrially. Hence, the best way to solve the γ-alumina structure is to consider the chemical process involved during the synthesis and preparation of the support, that is, the calcination of the hydrated precursor (boehmite) [3,23–25]. As a consequence, the γ-alumina bulk structure used for the current study results from the topotactic transformation of boehmite; we take into account that it is energetically more favorable for some Al cations to occupy nonspinel sites [23–25], as also found by others [31]. In a recent investigation [30], the interaction of MoS_2 with the support is modeled by an exchange of S atoms with –OH groups at the edges of the active phase. On the one hand, such a simplified approach neglects the chemical varieties of the Brønsted Al–OH sites and of the Lewis basic Al–O–Al sites present at the surface of the γ-alumina. On the other hand, the question of the steric hindrance or of the geometric constraints imposed by the local structure of the surface may be overlooked. Up to now, no theoretical study has been able to account for the effect of HDS conditions on the stable states of the surface by including the chemical potential of sulfur. As a consequence, it remains difficult to obtain unambiguous insights from the available works.

Addressing the challenging question of the active phase–support interaction requires the deployment of the most accurate models for the support's surfaces. Indeed, as shown in the present paper, there are several combined effects (electronic, geometric, orientation) between the active phase and the support. As explained previously, we use the refined and robust model established recently for γ-alumina [23–25]. For anatase, we refer to our previous studies [26,27]. The surface chemical species and thus the acid-basic properties have been quantitatively correlated with the sulfo-reductive conditions (p_{H_2}, p_{H_2S}, p_{H_2O}, and T) and the type of surface exposed by the support. The γ-alumina (110) surface is found to be highly hydroxylated, and the anatase (001) surface is hydroxylated and partially sulfided [27]. The two surfaces exhibit Brønsted sites under HDS conditions. In contrast, the γ-alumina (100) and the anatase (101) surfaces are neither hydrated nor sulfided and thus exhibit mainly Lewis sites. These results reveal the distinct chemical behavior of the two supports, and these preliminary steps were necessary for the investigation of support effects on the HDS activity. To further explore these effects, the potential energy surface for the adsorption of relevant models of the MoS_2 active phase must be solved. To meet this challenging task with computational chemistry, we need to determine the stable active phase configurations and orientations induced by the formation of different bond types (iono-covalent, hydrogen bonds, electrostatic interactions) between the support and Mo_6S_n ($n = 10$ to 24) clusters representative of single layers of nanosized MoS_2. This choice is also justified by a recent X-ray absorption spectroscopy (XAS) study that has revealed that the majority of the active-phase particles in a catalyst in use under industrial conditions is made of single sheets of MoS_2 [32]. In the next section, the methodology used for calculating Gibbs free energies of supported clusters is explained. Section 3.1 focuses on the results obtained on the isolated clusters, Sections 3.2 and 3.3 are devoted to Mo_6S_n clusters supported on γ-alumina and anatase, respectively. In Section 3.4, we propose a new approach where we extrapolate our results to larger sizes by including van der Waals contributions. In the discussion, we furnish new arguments to explain the effects of anatase and γ-alumina on HDS activity.

2. Methodology

Total energy calculations were performed within the density functional theory (DFT) and the generalized gradient approximation (GGA) of Perdew and Wang [33]. To solve the Kohn–Sham equations, we use the Vienna ab initio Simulation Package (VASP) [34]. The electronic convergence criterion is fixed at 0.1 meV per cell. The eigenstates of the electron wave functions are expanded on a plane-wave basis set, with pseudopotentials used to describe the electron–ion interactions within the projector augmented waves (PAW) approach [35]. For total energy calculations, we use a cutoff energy of 258.7 eV. According to the enlarged supercell sizes within the surface plane (with respect to [27]), the Brillouin zone sampling can be reduced at the Γ-point only. In the direction perpendicular to the surface, the slab thickness is decreased to keep system sizes within reach of DFT calculations (up to 250 atoms per supercell). The geometry optimization is carried out by calculation of the Hellmann–Feynman forces and an energy convergence criterion of 1 meV.

In the same spirit as for the MoS_2 active phase [18,19], and for the support surfaces [27], the thermodynamic model based on the chemical potential of sulfur, $\Delta\mu_S$, as the main thermodynamic variable bridges the gap between 0 K DFT calculations and the gas-phase conditions (p_{H_2}, p_{H_2S}, and T). The values of $\Delta\mu_S$ as a function of T and p_{H_2S}/p_{H_2} are given by the diagram of Fig. 1, so that the reader can more easily convert $\Delta\mu_S$ (used in the text) into reaction conditions. For the current study, the MoS_2 active phase is represented by triangular Mo_6S_n clusters exposing Mo-edges with various S-coverages similar to those described by Schweiger et al. in [19]. The isolated Mo_6S_n clusters are described in Section 3.1. The slab models representing the surfaces exhibit the stable hydroxylation and sulfidation states determined in one of our earlier papers [27]. In the present work, the reaction conditions explored correspond to a temperature range between 600 and 700 K and a water

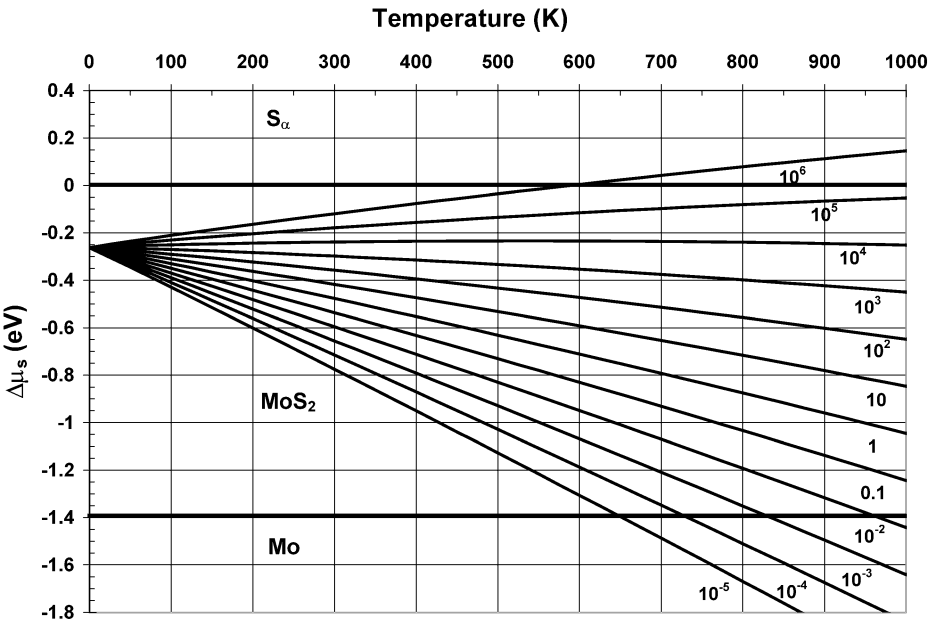

Fig. 1. $\Delta\mu_S$ values as a function of temperature and p_{H_2S}/p_{H_2} ratio (i.e., $\Delta\mu_S = h_{H_2S}(T) - h_{H_2}(T) - E_{S_\alpha} - T[s_{H_2S}(T) - s_{H_2}(T)] + RT\ln(p_{H_2S}/p_{H_2})$ as explained in previous works [17,19]). The domain where the MoS_2 bulk phase is stable: $-1.38 \leqslant \Delta\mu_S \leqslant 0$ eV. The reaction conditions explored in the present work are for T between 600 and 700 K.

partial pressure of 0.01 bar. This implies that the chemical species at the support surface is kept unchanged for the range of H_2S and H_2 partial pressures investigated.

The adhesion energy of the Mo_6S_n clusters on the (hkl) surface of the support is defined by

$$E_{adh/hkl} = E_{Mo_6S_n/hkl} - E_{hkl} - E_{Mo_6S_n}, \quad (1)$$

where $E_{Mo_6S_n/hkl}$ stands for the total energy of the Mo_6S_n cluster adsorbed on the (hkl) surface, E_{hkl} is the total energy of the (hkl) surface, and $E_{Mo_6S_n}$ is the reference energy of the isolated Mo_6S_n cluster. The adhesion energy is negative for an exothermic process.

The geometries of the Mo_6S_n clusters and of the two outermost atomic layers of the supports are optimized. Since the cluster is adsorbed on one side of the slab, corrections for dipole–dipole interactions are included.

The Gibbs free energy of the Mo_6S_n cluster adsorbed on the support (hkl) surface is given by the following relationship, when expressed with respect to the bulk MoS_2 phase

$$\Delta G_{Mo_6S_n/hkl} = \Delta G_{MoS_2} + \Gamma_{Mo_6S_n/hkl}, \quad (2)$$

where

$$\Gamma_{Mo_6S_n/hkl} = \Gamma_0(Mo_6S_n) + \frac{1}{6}E_{adh/hkl} - \frac{n-12}{6}\Delta\mu_S. \quad (3)$$

ΔG_{MoS_2} represents the Gibbs free energy of the MoS_2 bulk phase (−2.76 eV/Mo). $\Gamma_{Mo_6S_n/hkl}$ represents the energy required to create the Mo-edges of the cluster: it is positive and is expressed in eV per Mo-edge atom, so that it can be compared with edge energies calculated in our previous work [19]. Because the size of the cluster is fixed in Sections 3.1–3.3, ΔG_{MoS_2} is constant and the variation of $\Delta G_{Mo_6S_n/hkl}$ depends on $\Gamma_{Mo_6S_n/hkl}$. In what follows, we focus on the values taken by $\Gamma_{Mo_6S_n/hkl}$ and call them Gibbs free energy values (being aware that $\Gamma_{Mo_6S_n/hkl}$ represents the positive part of the Gibbs free energy of the cluster). Γ_0 (also expressed per Mo-edge atom) is the energy required to create the Mo-edges of the isolated cluster at $\Delta\mu_S = 0$. $\Delta\mu_S$ is the chemical potential of sulfur, depending on T and p_{H_2S}/p_{H_2}, as defined in [19]. Fig. 1 gives the $\Delta\mu_S$ values for different T and p_{H_2S}/p_{H_2} conditions.

The lowest values of $\Gamma_{Mo_6S_n/hkl}$ determine the stable adsorption configuration of the Mo_6S_n clusters as a function of the sulfo-reductive conditions.

To determine $E_{adh/hkl}$, numerous configurations for the adsorbed cluster were tested. The parallel orientation involves H-bonds and/or weak electrostatic interactions between the Mo_6S_n basal plane and the support. Different types of perpendicular and tilted orientations were considered:

- Through one Mo-edge saturated by S atoms involving weak electrostatic interactions and/or H-bonds;
- Through one unsaturated Mo-corner atom involving single iono-covalent Mo–O–Al(Ti) or Mo–S–Ti bridges;
- Through the unsaturated Mo-edge atoms involving multiple iono-covalent Mo–O–Al(Ti) or Mo–S–Ti bridges (also called “edge-bonded” clusters).

The extrapolation of the results to cluster sizes requires the addition of the van der Waals contributions neglected within DFT, particularly for the parallel orientation. The

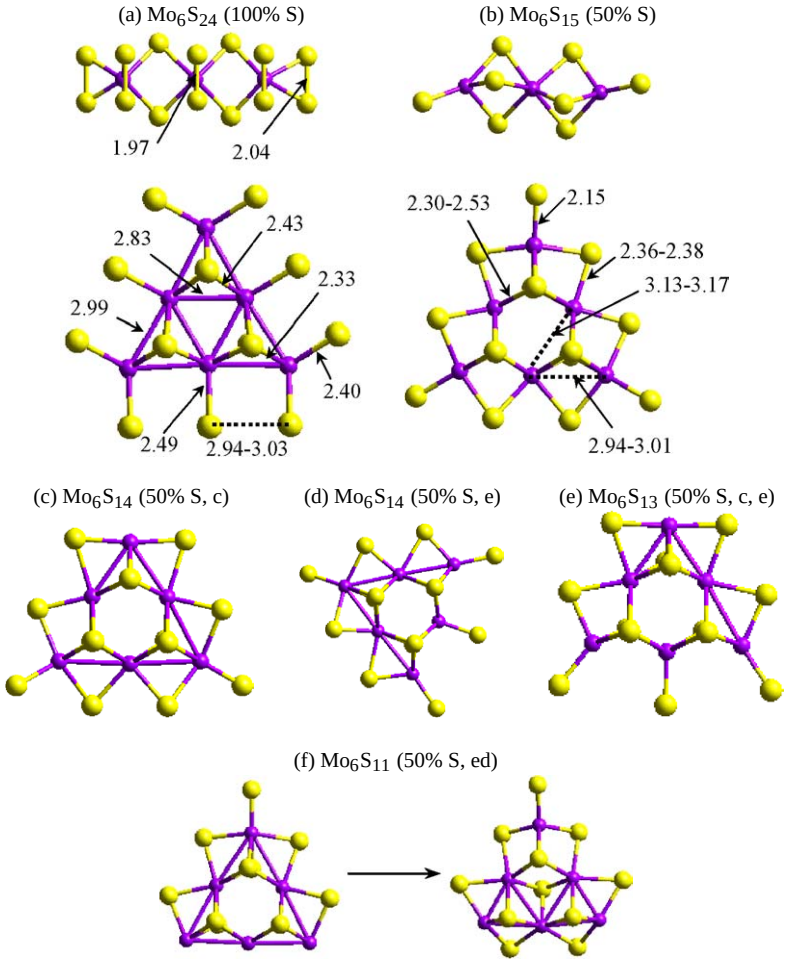

Fig. 2. Stoichiometry, optimized structures and notations for the different Mo_6S_n clusters (dark balls, molybdenum atoms; gray balls, sulfur atoms). (50% S, e) means 50% S-coverage at the edge with one edge vacancy, (50% S, c) 50% S-coverage at the edge with one corner vacancy, (50% S, ed) two edges with 50% S and 3 S-vacancies at the third edge (all distances in Angstrøm).

contributions were considered with the use of an approach based on a force-field methodology detailed in Section 3.4.

3. Results

3.1. Isolated Mo_6S_n clusters

We chose relevant triangular Mo_6S_n clusters exposing Mo-edges with relevant S-coverages (100 and 50%) at the edge, while taking into consideration the presence of one, two, and three vacancies per edge. The structures and notations used for the clusters are given in Fig. 2. The Mo_6S_{24} cluster with 100% sulfur coverage (Fig. 2a) exhibits sixfold coordinated Mo atoms at the edge, and sulfur atoms at the edges and corners form S–S dimers, as already found in previous studies [16,17,19,22]. The external Mo–Mo distance becomes shorter (2.98–3.00 Å) than in the bulk. The Mo–S bonds of the basal μ_3-S linked to a Mo atom at the edge are close to the bulk distance (2.43 Å), and those linked to a Mo atom at the corner are shorter (2.33 Å). The external Mo–S distances of the S–S dimers are 2.40 Å at the corner and 2.49 Å at the edge. The internal Mo–Mo distances are slightly shorter (2.82 Å) than at the edges (2.99 Å).

When the sulfur coverage is 50%, the Mo_6S_{15} cluster exhibits edge S atoms in a bridge position with a twofold coordination (Fig. 2b). The coordination of Mo-edge atoms remains equal to 6, and at the corner it decreases to 5. The Mo–μ_2S distances (at the edge) are around 2.37 Å, and the Mo–μ_1S distance at the corner is shorter (2.15 Å), following the bond-order conservation law. The internal Mo–μ_3S distances are between 2.30 and 2.53 Å. The edge Mo–Mo distances remain close to those of the Mo_6S_{24} cluster, and the internal Mo–Mo distances expand when compared with the Mo_6S_{24} cluster (at 3.13 to 3.17 Å).

Those clusters can exhibit different numbers and locations for S-vacancies. The first vacancy (Mo_6S_{14}) can be located either at the corner (c) (Fig. 2c) or at the edge (e) (Fig. 2d). When a second vacancy is created, the Mo_6S_{13} cluster combines both edge and corner vacancies (Fig. 2e). We have also considered the case where three vacancies are located on the same edge (ed) as for the Mo_6S_{11} cluster

Table 1
Gibbs free energies of the isolated Mo_6S_n clusters (Γ_0 in eV per Mo edge-atom) and adhesion energies of the adsorbed clusters ($E_{adh/hkl}$ in eV per cluster) as a function of the orientation

Mo_6S_n (S-coverage)	n-12	Γ_0	Orientation	γ-Alumina		Anatase (TiO_2)	
				$E_{adh/100}$	$E_{adh/110}$	$E_{adh/101}$	$E_{adh/001}$
Mo_6S_{24} (100% S)	12	0.83	Parallel ∥	−0.19	−0.32	−0.19	−0.21
			Ortho ⊥	+0.01	−0.08	−0.13	−0.16
Mo_6S_{15} (50% S)	3	1.35	Parallel ∥	−0.18	−0.65	–	−0.17
			Ortho ⊥	−0.10	−0.78	–	−0.17
Mo_6S_{14} (50% S, e)	2	1.34	Parallel ∥	−0.17	−0.22	−0.22	−0.20
			Ortho ⊥	−0.09	−0.31	−0.21	−0.10
Mo_6S_{14} (50% S, c)	2	1.41	Parallel ∥	–	−0.22	–	–
							−1.40 (c via S)
			Ortho ⊥	−1.29	−1.60	−1.30	
							−1.03 (c via O)
			Tilted	–	−0.27	−1.60	−1.42
Mo_6S_{13} (50% S, c, e)	1	1.59	Parallel ∥	–	–	−0.81	−0.90
			Ortho ⊥	−1.36	−1.66	−1.66	−1.67
			Tilted	–	+0.25	−2.15	−1.89
Mo_6S_{11} (50% S, ed)	−1	1.83	Ortho ⊥	+1.58	−0.11	−0.90	−1.29
Mo_6S_{10} (50% S, ed, c)	−2	2.31	Ortho ⊥	+0.3	−1.61	−2.49	−2.43

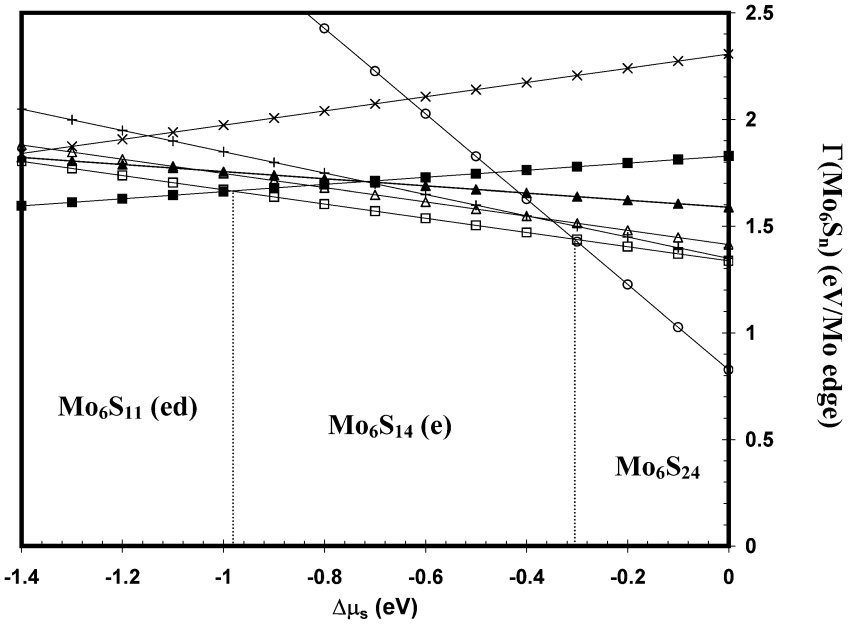

Fig. 3. Gibbs free energy diagram of the isolated Mo_6S_n clusters (positive part of the energy required for the creation of the cluster edges, see the text for explanation). ○, Mo_6S_{24} (100% S); +, Mo_6S_{15} (50% S); □, Mo_6S_{14} (50% S, e); △, Mo_6S_{14} (50% S, c); ▲, Mo_6S_{13} (50% S, e); ■, Mo_6S_{11} (50% S, ed); ×, Mo_6S_{10} (50% S, ed, c).

(Fig. 2f). In this case, the isolated cluster strongly reconstructs. As a result of their small sizes, we expect that these clusters exhibit specific energetic and structural properties, when compared with our previous work [19].

The Gibbs free energies of the different clusters for $\Delta\mu_S = 0$ are listed in Table 1. The diagram in Fig. 3 shows that for $\Delta\mu_S$ greater than −0.32 eV (i.e., $p_{H_2S}/p_{H_2} > 2 \times 10^3$), the Mo_6S_{24} cluster with 100% sulfur at the edge is the stable structure. For $\Delta\mu_S$ smaller than −0.32 eV, the more reductive conditions imply that the Mo_6S_{14} (e) cluster with 50% sulfur and one vacancy at the edge is stabilized. For $\Delta\mu_S$ values between −0.32 and −1.00 eV (i.e., $4 \times 10^{-3} < p_{H_2S}/p_{H_2} < 2 \times 10^3$, including usual HDS conditions), the Mo_6S_{14} (e) structure is more stable than the Mo_6S_{14} (c) cluster with the vacancy strictly located at the corner, and even more stable than the Mo_6S_{15} cluster (without S-vacancy). At this stage, it is worth comparing our results with previous studies carried out on larger clusters exhibiting nine Mo atoms per edge. One striking result obtained by Schweiger et al. in [19] was that one

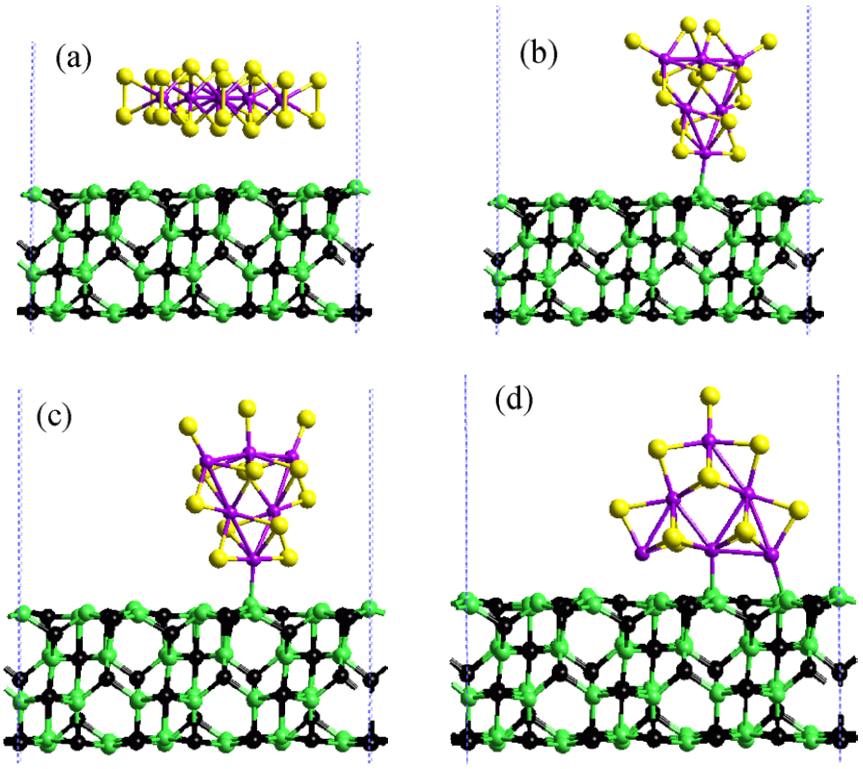

Fig. 4. Optimized structures of (a) $Mo_6S_{24}\|$, (b) $Mo_6S_{14}\perp$, (c) $Mo_6S_{13}\perp$, (d) $Mo_6S_{11}\perp$ adsorbed on the γ-alumina (100) surface. For the alumina slab: black balls, aluminum atoms; dark gray balls, oxygen atoms; white balls, hydrogen atoms. For the Mo_6S_n clusters: dark balls, molybdenum atoms; gray balls, sulfur atoms (the perpendicularly oriented clusters are anchored through Mo–O–Al bridges only).

S-vacancy located at the corner is stabilized under HDS conditions. For a small cluster, this effect seems to be enhanced, since one S-vacancy (as Mo_6S_{14}) remains the most stable configuration under a larger range of reaction conditions.

For smaller $\Delta\mu_S$ (< -1.00 eV), the stable cluster is Mo_6S_{11} with one missing row of edge S atoms. This structure is stabilized by a large reconstruction, where S-basal atoms migrate to the edge. Such a large reconstruction can only take place in small and isolated Mo_6S_n clusters, which explains why it was not found in previous studies [19].

3.2. Case of the γ-Al_2O_3 support

3.2.1. γ-Al_2O_3 (100) surface

We showed in [27] that the (100) surface is fully dehydroxylated for temperatures between 600 and 700 K, and for p_{H_2O} around 0.01 bar. For the range of p_{H_2S}/p_{H_2} corresponding to $\Delta\mu_S$ between -1.4 and 0 eV, no sulfidation occurs. As a consequence, the surface chemical state predicted for the (100) surface is the same as that calculated in [27] (see Fig. 4). The main structures of supported Mo_6S_n are given in Fig. 4, and their adhesion energies are listed in Table 1. The Gibbs free energy of supported Mo_6S_n clusters is given as a function of $\Delta\mu_S$ in Fig. 5. For $\Delta\mu_S$ greater than -0.24 eV (i.e., $p_{H_2S}/p_{H_2} > 9\times10^3$), the Mo_6S_{24} cluster with 100% S is stabilized in a parallel orientation with respect to the support. Only weak electrostatic interactions occur between the S-basal plane of the Mo_6S_{24} cluster and the (100) surface, leading to an exothermic adhesion energy of about -0.19 eV. The configuration changes into a perpendicular type for $\Delta\mu_S < -0.24$ eV, as the loss of S leads to the Mo_6S_{14} cluster. The energy cost for S-removal is balanced by the gain from the Mo–O bond formation, via one Mo–O–Al bridge. Such a cluster can be depicted as being in a "corner bonded" configuration. The cluster adhesion energy of -1.29 eV decreases the Mo_6S_{14} Gibbs free energy, permitting the stabilization of this cluster at a higher $\Delta\mu_S$ (less reducing conditions) than that observed for isolated clusters (vide supra). This result will be valid for all surfaces studied in this work. The optimized Mo–O bond length of the anchored cluster is 2.15 Å, and it remains compatible with EXAFS data of Leliveld et al. [6]. The Mo_6S_{13}(c) cluster ($E_{adh/100} = -1.36$ eV) is stabilized only for $\Delta\mu_S$ smaller than -0.98 eV, at the limit of the usual HDS conditions. Clusters exhibiting even more S-removal (such as Mo_6S_{11}(ed) with S-vacancies on one Mo-edge) are not stable under current sulfo-reductive conditions.

3.2.2. γ-Al_2O_3 (110) surface

For the aforementioned conditions, the (110) surface is hydrated with a hydroxyl coverage of 8.8 OH/nm^2, and it is not sulfided [27]. A slab model of the surface exhibiting the different types of hydroxyls is detailed in [24,25]. The main structures are depicted in Fig. 6, and their adhesion energies are listed in Table 1. The stable models are

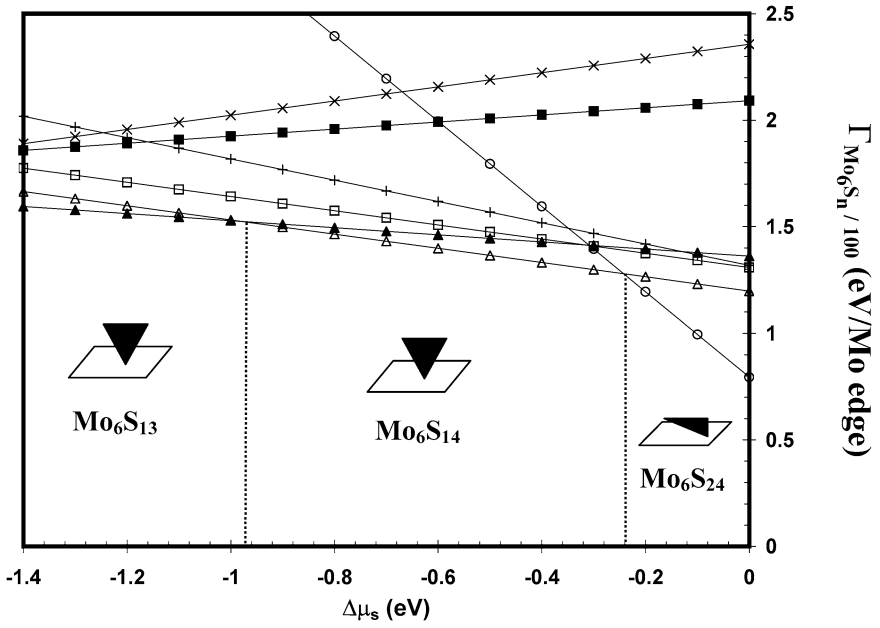

Fig. 5. Gibbs free energy diagram of the Mo_6S_n clusters adsorbed on the γ-alumina (100) surface. ○, Mo_6S_{24} (100% S, ∥); +, Mo_6S_{15} (50% S, ∥); □, Mo_6S_{14} (50% S, e, ∥); △, Mo_6S_{14} (50% S, c, ⊥); ▲, Mo_6S_{13} (50% S, c, e, ⊥); ■, Mo_6S_{11} (50% S, ed, ⊥); ×, Mo_6S_{10} (50% S, ed, c, ⊥).

given by the Gibbs free energy diagram in Fig. 7. Similarly to the (100) surface, the Mo_6S_{24} cluster with 100% sulfur is stable in a parallel orientation for high $\Delta\mu_S$. The adhesion energy (−0.32 eV) is slightly larger than for the (100) surface because of the formation of hydrogen bonds between the sulfur basal plane and the hydroxyls. A perturbation of the OH distribution can be seen, and the O–H stretching of about +0.006 Å for interacting hydroxyls may explain the OH stretching frequency shift observed in IR spectra [8,9]. Any proton transfer from the support to the edge S atom of the Mo_6S_{24} cluster is not stable.

More reductive conditions (a decrease in $\Delta\mu_S$) stabilize the perpendicular adsorption configuration of the Mo_6S_{14} cluster by creating one Mo–O–Al bridge with a Mo–O bond length of 2.26 Å, compatible with EXAFS data [6]. This is referred to as a corner bonded cluster. The O bridging atom is supplied by a formerly chemisorbed water molecule, transferring two protons to two neighboring O atoms (see Fig. 6b). This suggests a new interpretation of the IR spectrum [9]. The formation of a Mo–S–Al bridge for the Mo_6S_{15} cluster is less favorable than that of the Mo–O–Al bridge for the Mo_6S_{14} cluster, as shown by the more exothermic adhesion energy of −1.60 eV for the latter. As in the case of the (100) surface, the Mo_6S_{13} cluster ($E_{adh/110} = -1.66$ eV) is stable only for $\Delta\mu_S$ close to HDS conditions. It is important to note that even if the Mo_6S_{15} and Mo_6S_{14} clusters oriented in a parallel configuration are not stable, they do exhibit a significant adhesion energy (−0.78 eV for the Mo_6S_{15} cluster). In a similar way as for the Mo_6S_{24} cluster, this effect is explained by the hydrogen bonds between the hydroxyls and the S atoms of the clusters. Analysis of the orbitals close to the Fermi energy for the isolated Mo_6S_{24}, Mo_6S_{15}, and Mo_6S_{14} (Fig. 8) makes possible a qualitative understanding of the energy results. For the Mo_6S_{24} cluster, similarly to the earlier works [19,36], the occupied orbitals close to the Fermi level, located at the S-dimers (and represented by the dotted domains in Fig. 8a), are of σ_p character, giving rise to the out-of-registry protrusions observed in STM images. The energetically underlying orbitals are localized at the S-basal atoms; they contribute to hydrogen bonding with the surface hydroxyls. The electronic analysis of the Mo_6S_{15} cluster shows that the highest occupied bands are localized on all S atoms (at the edge and in the basal plane), as shown by Fig. 8b. These bands are available to contribute to the interaction with the hydrogen atoms of the surface hydroxyls. When one S-edge vacancy is created in Mo_6S_{14}, the orbitals at the basal S atoms neighboring the S-vacancy location have disappeared (Fig. 8c). This observation is consistent with previous results showing that for a 50% S coverage with one S-vacancy at the Mo-edge, the simulated STM image also reveals a loss of intensity of the bright spot localized at the S atom of the first S-sublayer of the basal plane [19]. Thus careful electronic analysis helps us to understand why the strongest adhesion energy for the parallel orientation is obtained for the Mo_6S_{15} cluster for which all S atoms exhibit orbitals at the Fermi level involved in the hydrogen bond interaction with the OH network of the (110) surface.

The Mo_6S_{11} and Mo_6S_{10} clusters are more stable than they are on the (100) surface, even if the corresponding $\Delta\mu_S$ value (< -1.40 eV) remains beyond realistic reaction conditions. The formation of multiple Mo–O–Al bridges along one Mo-edge is enhanced by the μ_1- or μ_2-OH species flexibility, which allows three Mo–O(H) bonds to be formed.

Finally, we have considered a peculiar configuration where the cluster interacts with multiple Mo–O–Al bridges

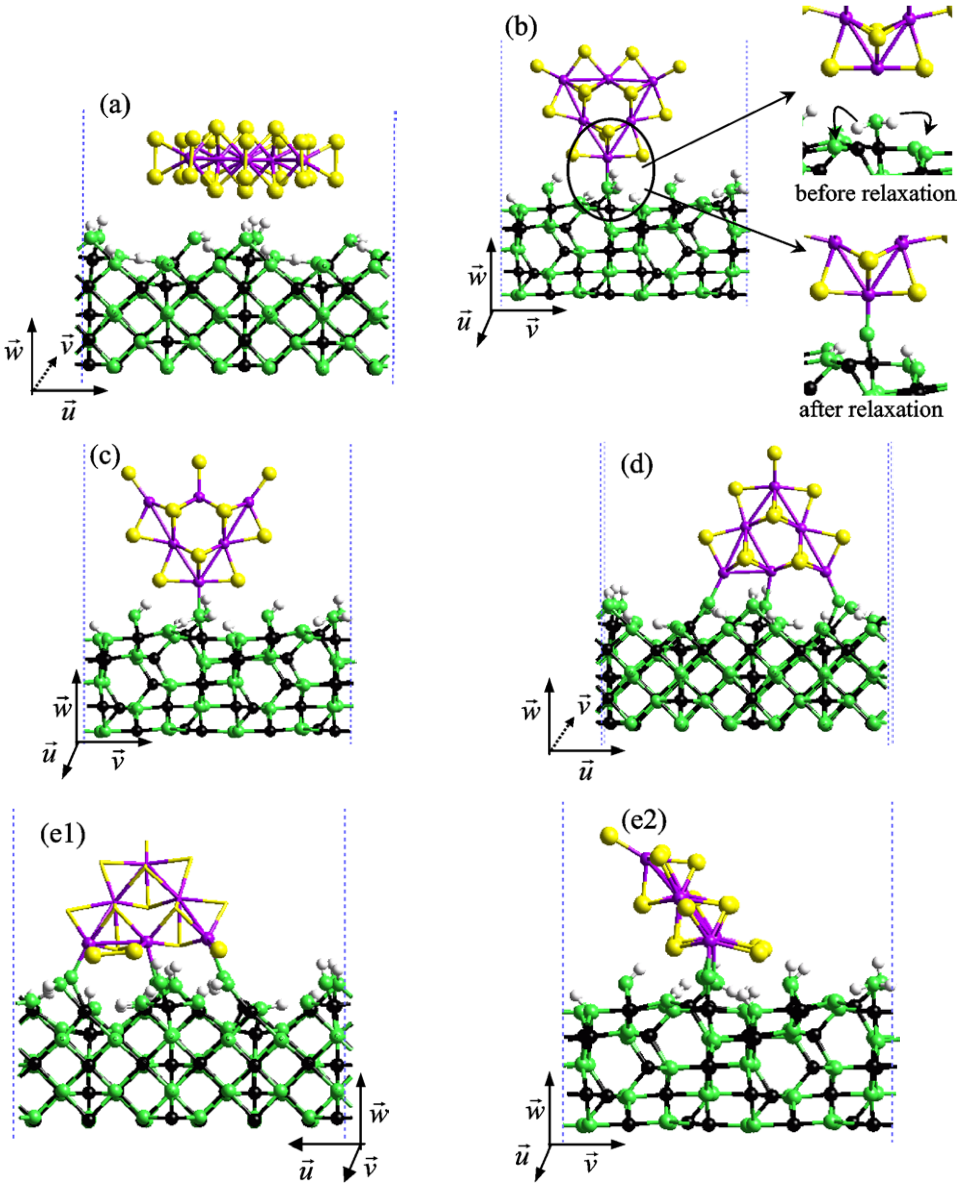

Fig. 6. Optimized structures of (a) Mo_6S_{24} ∥, (b) Mo_6S_{14} ⊥, (c) Mo_6S_{13} ⊥, (d) Mo_6S_{11} ⊥ adsorbed on the γ-alumina (110) surface. (e1) and (e2) represent two views of the tilted configuration of the Mo_6S_{14} cluster. (Same colors as in Fig. 4; the perpendicularly oriented clusters are anchored through Mo–O–Al bridges only.)

along one edge while still keeping S atoms present at this edge: the optimized Mo_6S_{14} clusters are represented in Figs. 6e1 and e2. The repulsive interactions of the S atoms on the Mo-edge with the O atoms cause the optimized edge-bonded cluster geometry to become tilted. The S atoms relax from the bridge into top positions at the interacting edge. A similar configuration is found for the optimized Mo_6S_{13} cluster. These steric constraints imply that the adsorption energies of the tilted clusters are endothermic or slightly exothermic (see Table 1). Hence, these configurations are not stabilized with respect to the stable Mo_6S_{14} adsorbed via one corner. We have similarly tested a tilted Mo_6S_{21} cluster exhibiting 100% S on two edges (as for Mo_6S_{24}) and 50% sulfur on the third edge linked to the support. This leads to similar conclusions: for the same reaction conditions, the stable cluster prefers to lie parallel with a higher degree of sulfidation (Mo_6S_{24}). For the sake of clarity, we have not reported the tilted configurations in Fig. 7.

On γ-alumina, these results demonstrate that multiple Mo–O–Al bridges involving the Mo-edge cannot stabilize clusters in tilted or in perpendicular configurations. For the same HDS conditions, the clusters will be preferentially anchored to the support through one corner Mo-atom (“corner bonded”). The role of the hydrogen bond network at the support’s surface is crucial for a correct evaluation of the energy of the system. The local flexibility of the OH– network is not available on the rigid μ_3-O square network of the dehydrated (100) surface. It can be understood why previous

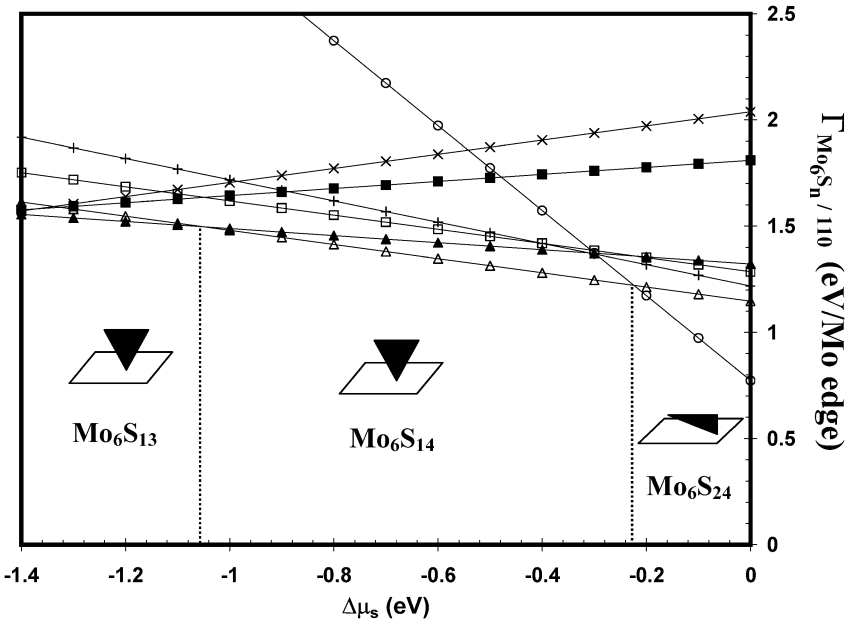

Fig. 7. Gibbs free energy diagram of the Mo_6S_n clusters adsorbed on the γ-alumina (110) surface. ○, Mo_6S_{24} (100% S, ∥); +, Mo_6S_{15} (50% S, ⊥); □, Mo_6S_{14} (50% S, e, ⊥); △, Mo_6S_{14} (50% S, c, ⊥); ▲, Mo_6S_{13} (50% S, c, e, ⊥); ■, Mo_6S_{11} (50% S, ed, ⊥); ×, Mo_6S_{10} (50% S, ed, c, ⊥).

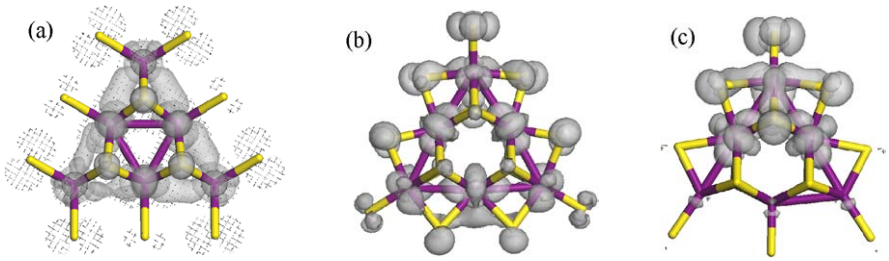

Fig. 8. Highest occupied bands for the (a) Mo_6S_{24} cluster in the range of [−0.53 eV; 0] (the dotted regions correspond to the highest energy interval [−0.31 eV; 0]); (b) Mo_6S_{15} clusters close to Fermi energy [−0.12 eV; 0] eV; (c) Mo_6S_{14} very close to the Fermi energy (lower occupied bands are below −0.6 eV).

studies [28–30] were not able to capture such subtle effects that depend precisely on the local structure of the support.

3.3. Case of the anatase support

3.3.1. Anatase (101) surface

The (101) surface of anatase is dehydrated and not sulfided according to [27]. The structures and adhesion energies are given in Fig. 9 and Table 1, respectively. Fig. 10 shows that for $\Delta\mu_S$ greater than −0.21 eV, the parallel configuration (Fig. 9a) is again the most stable.

The main striking difference with γ-alumina is that the edge-bonded Mo_6S_n ($10 \leqslant n \leqslant 14$) clusters are stabilized for $\Delta\mu_S$ below −0.21 eV. Furthermore, the $Mo_6S_{14} \rightarrow Mo_6S_{13}$ transition occurs on this surface for a significantly higher value of $\Delta\mu_S$ (−0.50 eV) than it does on alumina, because of the high exothermic adhesion energy of the Mo_6S_{13} cluster, −2.15 eV (Table 1). As shown in Figs. 9b and c, there is an epitaxial relationship between the anatase (101) surface and the Mo-edge that permits the formation of multiple Mo–O–Ti and Mo–S–Ti bridges. As highlighted in Fig. 9b, the four-member Mo–S–Ti–O–Mo rings of the adsorbed Mo_6S_{14} and Mo_6S_{13} clusters mimic the Ti–O–Ti–O–Ti ring of the anatase bulk within the ($\boldsymbol{v}$, $\boldsymbol{w}$) plane. The stable Mo_6S_{14} and Mo_6S_{13} clusters are tilted: the plane of the Mo atoms exhibits an angle of 52° with respect to the anatase surface. Such a tilted orientation is induced by the formation of the Mo–S–Ti–O–Mo rings. This result may explain why EXAFS reveals a higher Mo–O coordination number on anatase than on alumina [6], and why tilted orientations have been observed on this support in electron microscopy experiments [37,38]. Furthermore, the Mo–O–Ti bridges exhibit Mo–O lengths between 1.98 and 2.10 Å, which is also compatible with EXAFS data [6]. The optimized Ti–S bond lengths are between 2.38 and 2.51 Å. It must be stressed that the regular surface O–O and Ti–Ti spacing (3.80 Å) along the $\boldsymbol{u}$ direction does not perfectly match the Mo–Mo distance (3.16 Å) of the Mo-edge. For small clusters, the relaxation effects of the surface O atoms and of the Mo atoms compensate for the mismatch; however, it may be expected that for large clusters (where relaxation effects are reduced), the perfect epitaxial relationship along the $\boldsymbol{u}$ direction will not be maintained.

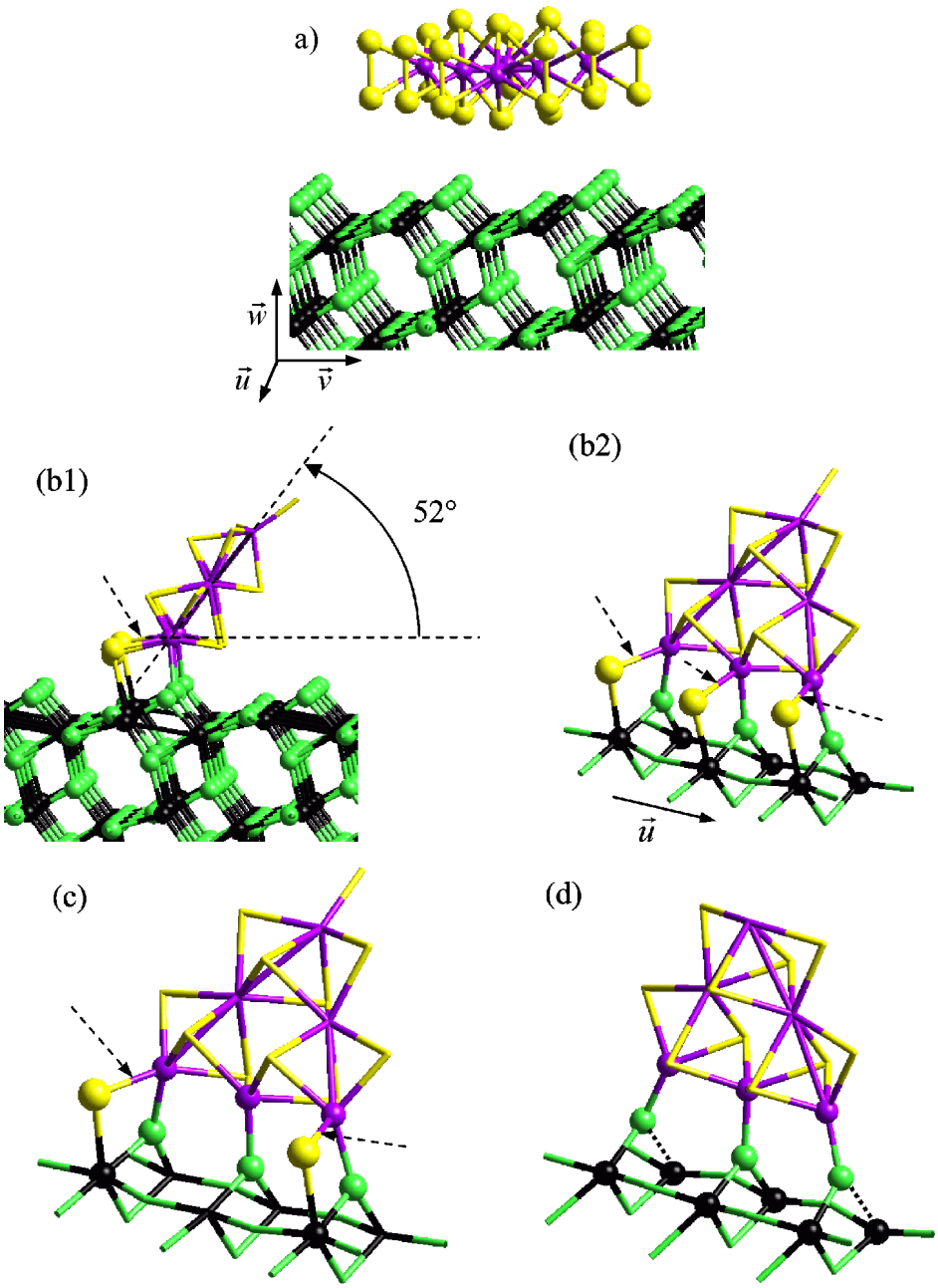

Fig. 9. Optimized structures of (a) Mo_6S_{24} ∥; (b1) and (b2) Mo_6S_{14} tilted; (c) Mo_6S_{13} tilted; (d) Mo_6S_{10} ⊥ adsorbed on the anatase (TiO_2) (101) surface. For the titania slab: black balls, titanium atoms; dark gray balls, oxygen atoms; white balls, hydrogen atoms. For the Mo_6S_n clusters: dark balls, molybdenum atoms; gray balls, sulfur atoms. (The tilted clusters are anchored through Mo–O–Al and/or Mo–S–Ti bonds (the latter are indicated by arrows).)

For $\Delta\mu_S$ less than −1.32 eV, the stable Mo_6S_{10} clusters interact perpendicularly via multiple Mo–O–Ti bridges (Fig. 9d). The Mo_6S_{10} anchorage leads to a strong adhesion energy of −2.49 eV. For the γ-alumina surfaces, such an epitaxial relationship is not possible, which explains why the Mo-edge-bonded clusters in a perpendicular or tilted configuration are not stable.

3.3.2. *Anatase (001) surface*

The (001) surface is hydroxylated and partially sulfided, with a hydroxyl coverage of 3.46 OH/nm^2 and a S-coverage of 1.73 S/nm^2 [27]. The structures and adhesion energies are given in Fig. 11 and Table 1.

It is important to note that the hydroxyl concentration of the (001) surface is less than twice that of the alumina (110) surface, which reduces the stabilization by hydrogen bonding for parallel orientation. Hence, the adhesion energies of such configurations are significantly lower than they are for alumina. For the Mo_6S_{15} cluster, the adhesion energy is about 3 times smaller (Table 1). This difference will play a role when the larger size cluster is considered in the next section.

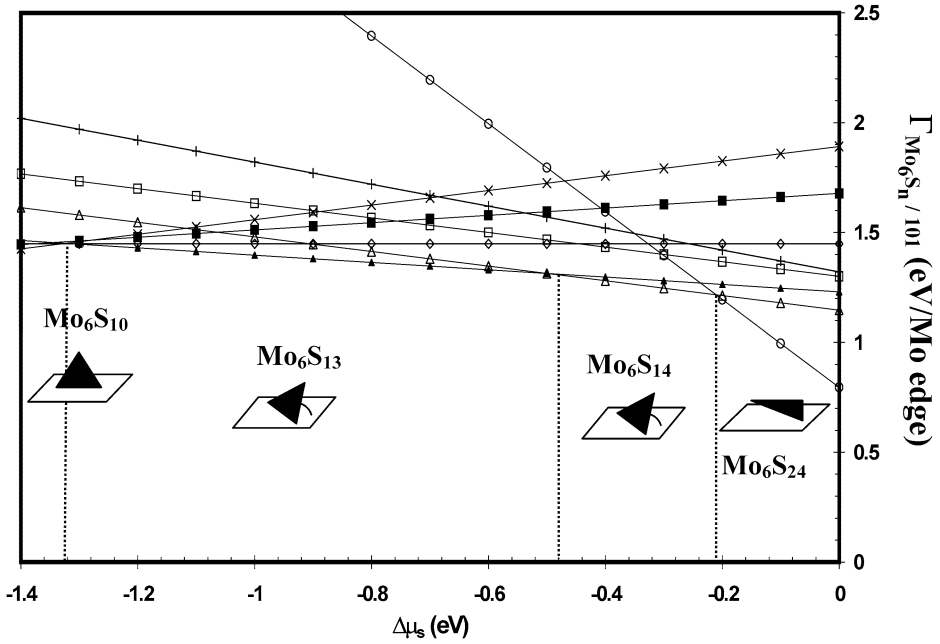

Fig. 10. Gibbs free energy diagram of the Mo_6S_n clusters adsorbed on the anatase (TiO_2) (101) surface. ○, Mo_6S_{24} (100% S, ∥); +, Mo_6S_{15} (50% S, ∥); □, Mo_6S_{14} (50% S, e, ∥); △, Mo_6S_{14} (50% S, e, tilted); ▲, Mo_6S_{13} (50% S, c, e, tilted); ◇, Mo_6S_{12} (50% S, c, c, e, tilted); ■, Mo_6S_{11} (50% S, ed, ⊥); ×, Mo_6S_{10} (50% S, ed, c, ⊥).

The stronger stabilization of the Mo_6S_{13}, Mo_6S_{11}, and Mo_6S_{10} clusters versus γ-alumina is also observed for this surface (see Fig. 12). The strong Mo_6S_{13} adhesion energy induces a high $\Delta\mu_S$ value for the $Mo_6S_{14} \rightarrow Mo_6S_{13}$ transition. As for the (101) surface, the tilted orientations not only involve Mo–O–Ti, but also Mo–S–Ti bridges, and maximize the number of Mo–S–Ti bridges with the support (Fig. 11b). An epitaxial relationship between the (001) surface and the Mo-edge structure also exists. However, there is a slight difference with the (101) surface because of the sulfidation state of the (001) surface, which implies that two types of four-membered rings ensure the cluster-support interface: Mo–S–Ti–S–Mo and Mo–O–Ti–O–Mo rings. The two types of Mo–S bond lengths are about 2.23 and 2.46 Å, the Ti–S bond lengths are about 2.60–2.64 Å, and the Mo–O lengths 2.11 and 2.30 Å. When compared with the (101) surface, the angle between the Mo atom plane and the surface increases to 71° (Fig. 11b).

Finally, the Mo_6S_{11} cluster is stable for $\Delta\mu_S$ less than −1.02 eV. The configurations shown in Fig. 11c reveal that the central edge Mo atom is in a bridging position between two O atoms, and the two other corner Mo atoms are linked with the S atoms of the surface. The two Mo–S bond lengths of the Mo–S–Ti bridges are about 2.31 Å, and the Mo–O lengths are 2.17 and 2.29 Å.

3.4. Extrapolation for larger clusters and size effects

3.4.1. Description of the model used

The results obtained in the previous sections concern Mo_6S_n clusters exhibiting three atoms per edge. This corresponds to a particle size of about 6 Å (if one considers the edge length as the relevant cluster size), which is smaller than the sizes observable by electron microscopy. For such small clusters, the van der Waals interactions remain negligible. However, mean sizes observed by HREM are about 20–30 Å, according to Mo loading [39]. As a consequence, it is useful to propose an approach for the extrapolation of our DFT results for larger sizes. Furthermore, such an approach requires to account for the effect of the long-range interactions between correlated charge fluctuations, which are underestimated in the DFT formalism. Two well-known cases show that DFT fails in the description of van der Waals interactions: the first is the adsorption of paraffins in zeolites [40], and the second is the description of layered systems such as MoS_2 itself [41]. Similarly, the van der Waals interactions between the basal S atom layer in the MoS_2 systems and the O atom network of the supports are expected to modify the energetic results for large particle sizes. It is not yet possible to carry out a consistent treatment of the van der Waals contributions in the DFT formalism. Thus, as means of estimating the long-range effects, we use two different force fields: the Universal Force Field (UFF) [42] and Compass [43], as delivered within the Cerius^2 interface [44]. UFF contains Lennard–Jones fitted parameters for the Mo, Al, O, and S elements, and the Compass force field does not contain available parameters for the Mo element. In the latter case, the MoS_2 cluster is modeled by S atoms only at the same position as found in MoS_2. For the parallel orientations, we have first determined the distance of the MoS_2 layer to the oxide surface at the energy minimum of the system. We have carried out this approach for clusters exhibiting 3 Mo per edge (as in the previous sections) and for a large cluster with 9 Mo atoms per edge (45 Mo atoms and 99 S atoms). The

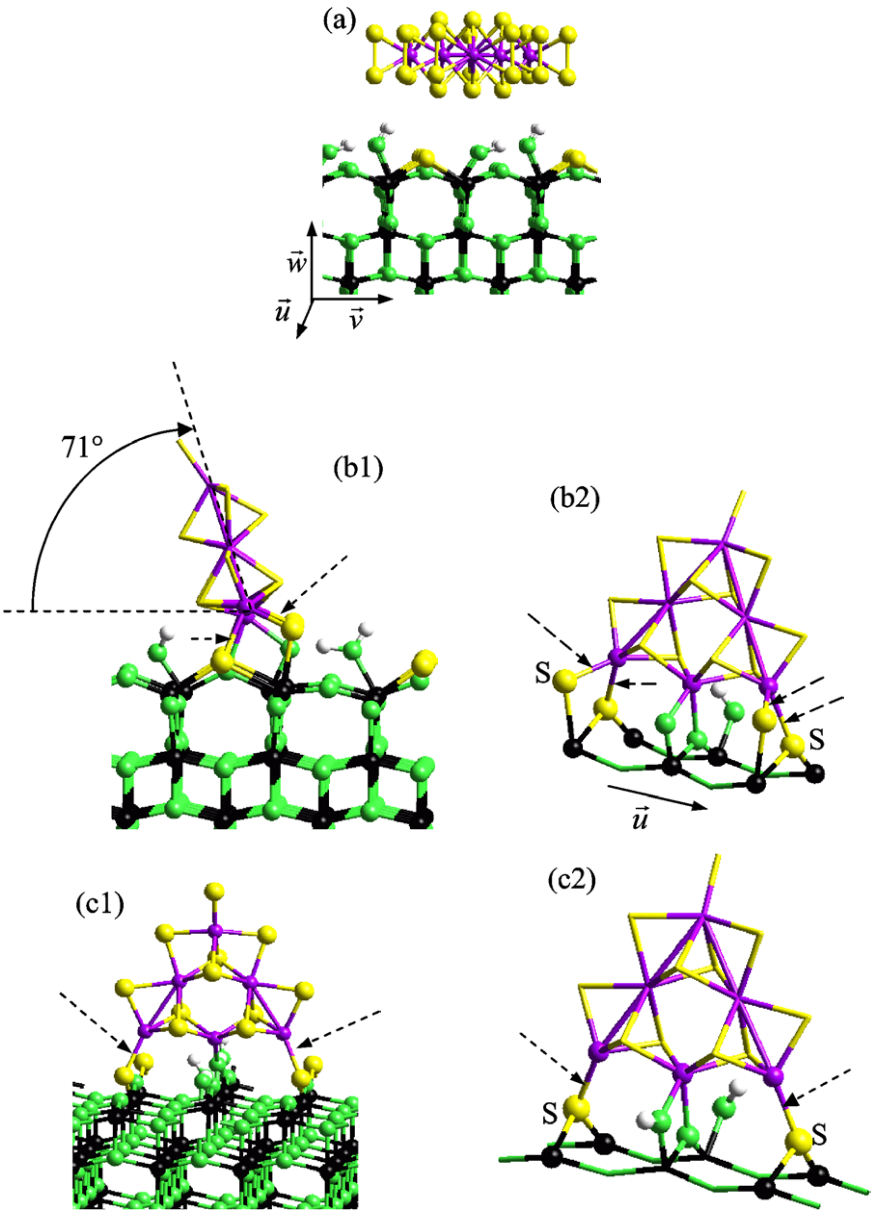

Fig. 11. Optimized structures of (a) Mo_6S_{24} ∥; (b1 and b2) Mo_6S_{13} tilted; (c1 and c2) Mo_6S_{11} ⊥ adsorbed on the anatase (TiO_2) (001) surface (same colors as in Fig. 9). (The perpendicularly oriented and tilted clusters are anchored through Mo–O–Al and/or Mo–S–Ti bonds (the latter are indicated by arrows). The tilted Mo_6S_{14} cluster (not represented here) is similar to Mo_6S_{13} with two S-atoms at the corner.)

values found with Compass are reported in Table 2; they are rather consistent with the UFF results (a slightly larger value is found for UFF). The van der Waals contributions are thus expected to be less than 10 kJ/mol of basal S atoms and depend slightly on the type of oxide surface. This estimate seems to be reasonable when it is compared with the MoS_2 layer van der Waals binding energy found within the fully nonlocal functional formalism recently proposed by Rydberg et al. [41].

The S atoms mainly contributing to the van der Waals corrections are those of the first row of S atoms belonging to the basal plane and directly facing the surface of the support. When considering the S atoms located at a greater distance, we observe that their contributions diminish drastically. Hence, we scale the van der Waals contributions with the number of S atoms belonging to the first row of basal S atoms. Such a consideration implies that the Gibbs free energy for the different types of clusters (including various

Table 2
Van der Waals corrections (in eV per S-atom) used for large MoS_2 clusters on alumina and anatase located at the equilibrium distance D_0 of the outermost oxygen plane of the support

Surface (*hkl*)	D_0 (Å)	E_{adh}^{vdw} (eV/S)
Alumina (100)	3.00	−0.10
Alumina (110)	2.00	−0.07
Anatase (101)	2.50	−0.08
Anatase (001)	3.00	−0.06

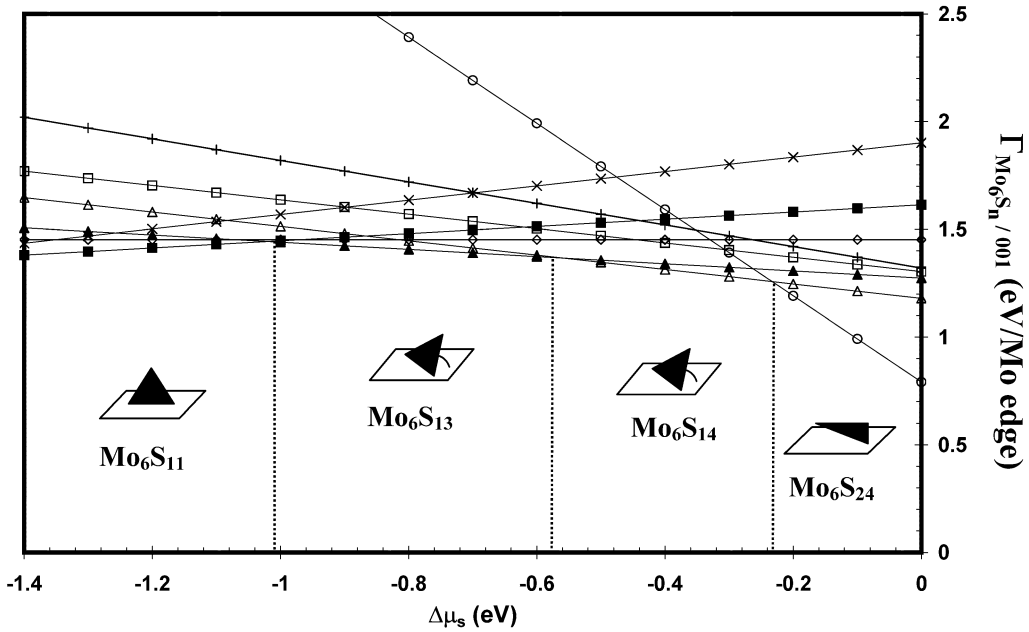

Fig. 12. Gibbs free energy diagram of the Mo_6S_n clusters adsorbed on the anatase (TiO_2) (001) surface. ○, Mo_6S_{24} (100% S, ∥); +, Mo_6S_{15} (50% S, ∥); □, Mo_6S_{14} (50% S, e, ∥); △, Mo_6S_{14} (50% S, c, ⊥); ▲, Mo_6S_{13} (50% S, c, e, tilted); ◇, Mo_6S_{12} (50% S, c, c, e, tilted); ■, Mo_6S_{11} (50% S, ed, ⊥); ×, Mo_6S_{10} (50% S, ed, c, ⊥).

S-coverages) can be written as a function of the size represented by the k number of Mo per edge.

In the case of a parallel oriented cluster with Mo-edges covered by 100% S, the stoichiometry is $Mo_{k(k+1)/2}S_{k(k+5)}$. By analogy with Eqs. (2) and (3), the Gibbs free energy (per Mo-edge atom) is

$$\Delta G(\mathrm{Mo}_{k(k+1)/2}\mathrm{S}_{k(k+5)}) = \frac{k(k+1)/2}{3k-3}\Delta G(\mathrm{MoS_2}) + \Gamma(\mathrm{Mo}_{k(k+1)/2}\mathrm{S}_{k(k+5)}), \quad (4)$$

$$\Gamma(\mathrm{Mo}_{k(k+1)/2}\mathrm{S}_{k(k+5)}) = \Gamma_0(\mathrm{Mo_6S_{24}}) + \frac{N_S^{\mathrm{DFT}}}{3k-3}\frac{E_{\mathrm{adh}}^{\mathrm{DFT}}(\mathrm{Mo_6S_{24}})}{12} + \frac{N_S^{\mathrm{vdw}}}{3k-3}E_{\mathrm{adh}}^{\mathrm{vdw}} - \frac{4k}{3k-3}\Delta\mu_S, \quad (5)$$

where

$$N_S^{\mathrm{DFT}} = N_S^{\mathrm{vdw}} = k(k-1)/2 + 3k. \quad (6)$$

The bulk energy part of the Gibbs free energy depends on the cluster size. In particular, the expected trend is that the stability of the cluster increases with the size. Because we focus on the comparison of different supports and cluster configurations for the same cluster size, we consider only the variation in Γ (also called Gibbs free energy) in what follows. In contrast, if we wanted to compare clusters of different sizes, the bulk term should be included. As for the Mo_6S_{24} cluster, $\Gamma_0(Mo_6S_{24})$ and Γ represent the energies required to create the cluster edges of the isolated and adsorbed clusters, respectively. $E_{\mathrm{adh}}^{\mathrm{DFT}}/12$ is the DFT adhesion energy per S-edge atom obtained from the Mo_6S_{24} cluster, and $E_{\mathrm{adh}}^{\mathrm{vdw}}$ is the van der Waals adhesion energy per S atom. N_S^{vdw} and N_S^{DFT} are the scaling numbers for the S atoms involved in the van der Waals and DFT contributions, respectively. To the S-basal atoms is added the contribution of one-half of the S atoms belonging to the S-dimers located at the edge. N_S^{vdw} and N_S^{DFT} are proportional to k^2. The fourth term corresponds to the effect of the sulfur chemical potential term resulting from the stoichiometry changes. As a consequence, and according to Eq. (5), the Gibbs free energy of such clusters decreases as a function of size k, because of the van der Waals and H-bond attractive interactions.

In the case of a Mo-edge cluster covered by 50% S at the edge adsorbed in a parallel orientation, the expression becomes

$$\Gamma(\mathrm{Mo}_{k(k+1)/2}\mathrm{S}_{k(k+2)}) = \Gamma_0(\mathrm{Mo_6S_{15}}) + \frac{N_S^{\mathrm{DFT}}}{3k-3}\frac{E_{\mathrm{adh}}^{\mathrm{DFT}}(\mathrm{Mo_6S_{15}})}{12} + \frac{N_S^{\mathrm{vdw}}}{3k-3}E_{\mathrm{adh}}^{\mathrm{vdw}} - \frac{k}{3k-3}\Delta\mu_S, \quad (7)$$

where

$$N_S^{\mathrm{DFT}} = k(k-1)/2 + 3k \quad \text{and} \quad N_S^{\mathrm{vdw}} = k(k-1)/2. \quad (8)$$

The differences with Eqs. (5) and (6) come from the stoichiometry of the clusters and from the number of sulfur atoms involved in the van der Waals correction (the basal atoms only). For the same reason as in the previous case, the Gibbs free energy (expressed per Mo-edge atom) decreases as a function of k, because of the van der Waals and H-bond attractive interactions.

In the case of a Mo-edge cluster covered by 50% S at the edge plus one S-vacancy and adsorbed in a parallel orientation, the expression becomes

$$\Gamma(\mathrm{Mo}_{k(k+1)/2}\mathrm{S}_{k^2+2k-1}) = \Gamma_0(\mathrm{Mo_6S_{14}}) + \frac{N_\mathrm{S}^\mathrm{DFT}}{3k-3}\frac{E_\mathrm{adh}^\mathrm{DFT}(\mathrm{Mo_6S_{14}})}{11} + \frac{N_\mathrm{S}^\mathrm{vdw}}{3k-3}E_\mathrm{adh}^\mathrm{vdw} - \frac{k-1}{3k-3}\Delta\mu_\mathrm{S}, \quad (9)$$

where

$$N_\mathrm{S}^\mathrm{DFT} = k(k-1)/2 + 3k - 1 \quad \text{and} \quad N_\mathrm{S}^\mathrm{vdw} = k(k-1)/2. \quad (10)$$

These expressions are very similar to the previous ones.

For the same cluster type adsorbed in a perpendicular orientation through one corner,

$$\Gamma(\mathrm{Mo}_{k(k+1)/2}\mathrm{S}_{k^2+2k-1}) = \Gamma_0(\mathrm{Mo_6S_{14}}) + \frac{N_\mathrm{S}^\mathrm{DFT}}{3k-3}E_\mathrm{adh}^\mathrm{DFT}(\mathrm{Mo_6S_{14}}) + \frac{N_\mathrm{S}^\mathrm{vdw}}{3k-3}E_\mathrm{adh}^\mathrm{vdw} - \frac{k-1}{3k-3}\Delta\mu_\mathrm{S}, \quad (11)$$

where

$$N_\mathrm{S}^\mathrm{DFT} = 1 \quad \text{and} \quad N_\mathrm{S}^\mathrm{vdw} = 4. \quad (12)$$

According to the corner anchoring, the four S atoms, in the coordination sphere of the Mo atom linked to the support, account for the van der Waals contributions. In this case, it is clear that the van der Waals and DFT adhesion energies of the support become negligible for large sizes, and the clusters behave as if they were isolated.

For a cluster adsorbed in a tilted configuration with an anchoring through one edge,

$$\Gamma(\mathrm{Mo}_{k(k+1)/2}\mathrm{S}_{k^2+k-1}) = \Gamma_0(\mathrm{Mo_6S_{14}}) + \frac{1}{6}E_\mathrm{adh}^\mathrm{DFT}(\mathrm{Mo_6S_{11}}) + \frac{N_\mathrm{S}^\mathrm{vdw}}{3k-3}E_\mathrm{adh}^\mathrm{vdw} - \frac{k-1}{3k-3}\Delta\mu_\mathrm{S}, \quad (13)$$

where

$$N_\mathrm{S}^\mathrm{vdw} = 2(k-1). \quad (14)$$

The van der Waals contribution scales linearly with the size of the edge ($N_\mathrm{S}^\mathrm{vdw}$ is proportional to k, that is, the number of the row of the basal S-atoms close to the edge). As a consequence, the van der Waals and the DFT adhesion energies exhibit a finite limit when the size increases.

For a cluster adsorbed in a perpendicular orientation with an anchoring through one edge,

$$\Gamma(\mathrm{Mo}_{k(k+1)/2}\mathrm{S}_{k^2+k-1}) = \Gamma_0(\mathrm{Mo_6S_{11}}) + \frac{1}{6}E_\mathrm{adh}^\mathrm{DFT}(\mathrm{Mo_6S_{11}}) + \frac{N_\mathrm{S}^\mathrm{vdw}}{3k-3}E_\mathrm{adh}^\mathrm{vdw} - \frac{1}{3k-3}\Delta\mu_\mathrm{S}, \quad (15)$$

where

$$N_\mathrm{S}^\mathrm{vdw} = 2(k-1). \quad (16)$$

3.4.2. Case of γ-Al_2O_3

On the alumina support, the first insight is that for a size above four Mo per edge (Fig. 13), the perpendicular orientation is no longer thermodynamically stable. The stable clusters in a parallel orientation are $Mo_{21}S_{66}$, $Mo_{21}S_{47}$, and, eventually, $Mo_{21}S_{48}$, according to the chemical potential of sulfur. At high chemical potential of sulfur, the cluster covered by 100% S of sulfur with dimers ($Mo_{21}S_{66}$) is stabilized, and under HDS conditions, the cluster with 50% S ($Mo_{21}S_{47}$) including one vacancy close to the corner can be stabilized. As already mentioned in Section 3.1, this result remains very close to the previous work by Schweiger et al. in [19] on isolated large triangular clusters, where it was found that under HDS conditions, the 50% coverage plus one vacancy close to the corner position is stabilized. For the highly hydroxylated (110) surface, the stability of parallel clusters such as $Mo_{21}S_{48}$ (without vacancy) is slightly enhanced versus $Mo_{21}S_{47}$ because of hydrogen bond interactions. In the case of the size $k = 6$, we thus observe that the Gibbs free energy of $Mo_{21}S_{48}$ is lower than that of $Mo_{21}S_{47}$. This never occurs on weakly hydrated surfaces. Finally, the straight lines representing the Gibbs free energies of the perpendicular configurations are significantly shifted to higher values in energy. The hydroxylated (110) surface is slightly more favorable for the perpendicular orientation because of the flexibility of the hydroxyl groups, which can relax more easily to fit with the Mo–Mo spacing of the MoS_2 phase. On the (100) surface the misfit of the O and Al surface network with the Mo-edge, together with the low S-affinity of alumina, destabilizes the perpendicular and tilted anchoring via the Mo-edge. Hence, only particles with a Mo-edge length smaller than 10 Å (i.e., a diameter of 20 Å, assuming hexagonal particles) can be thermodynamically stabilized in a perpendicular configuration bonded via one corner. Ongoing simulations of the S-edge interaction are intended to determine whether this effect is influenced by the type of edge exposed by the active phase.

3.4.3. Case of anatase

On the titania support, Fig. 14 shows that for the edge length $k = 6$ the perpendicular and tilted orientations remain stable. On the two anatase surfaces, our model shows that the edge-bonded clusters are thermodynamically stable up to $k = 14$ and for conditions close to HDS. This means that MoS_2 crystallites with an edge length smaller than 45 Å (i.e., a diameter of 90 Å for hexagonal particles) may exist in a perpendicular or tilted configuration, thanks to the epitaxial relationship between the Mo-edge and the anatase support. To a certain extent, this result may furnish an explanation of the electron microscopic observations of Sakashita

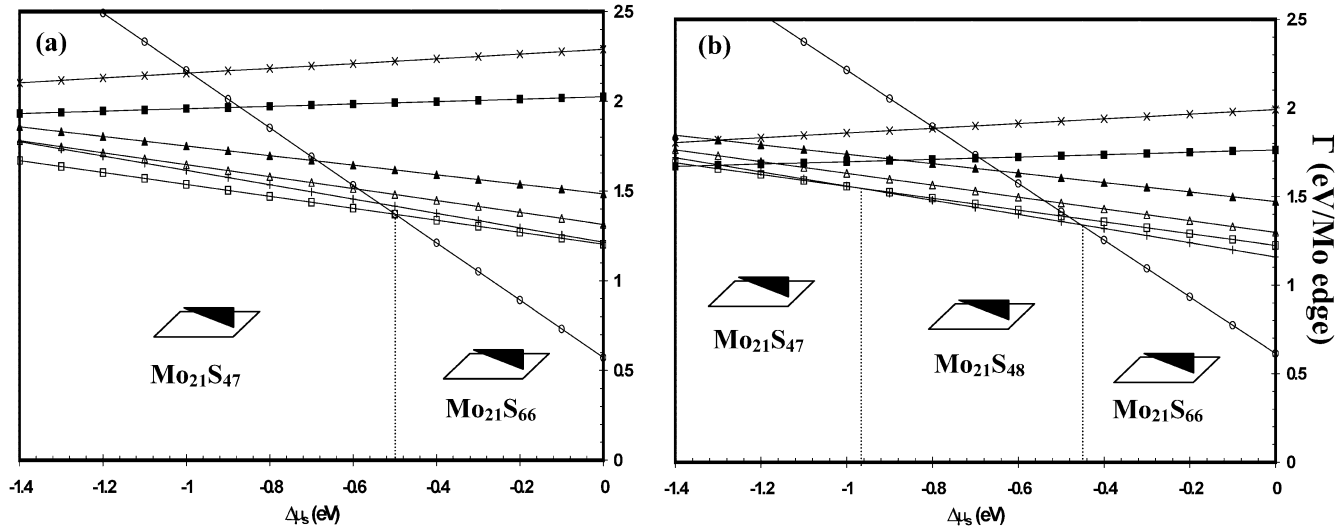

Fig. 13. Gibbs free energy diagrams of the MoS_2 clusters with $k = 6$ Mo per edge adsorbed on the γ-alumina: (a) (100) surface, (b) (110) surface. ○, $Mo_{21}S_{66}$ (100% S, ∥); +, $Mo_{21}S_{48}$ (50% S, ∥); □, $Mo_{21}S_{47}$ (50% S, e, ∥); △, $Mo_{21}S_{47}$ (50% S, c, ⊥); ▲, $Mo_{21}S_{46}$ (50% S, c, e, ⊥); ■, $Mo_{21}S_{41}$ (50% S, ed, ⊥); ×, $Mo_{21}S_{40}$, (50% S, ed, c, ⊥).

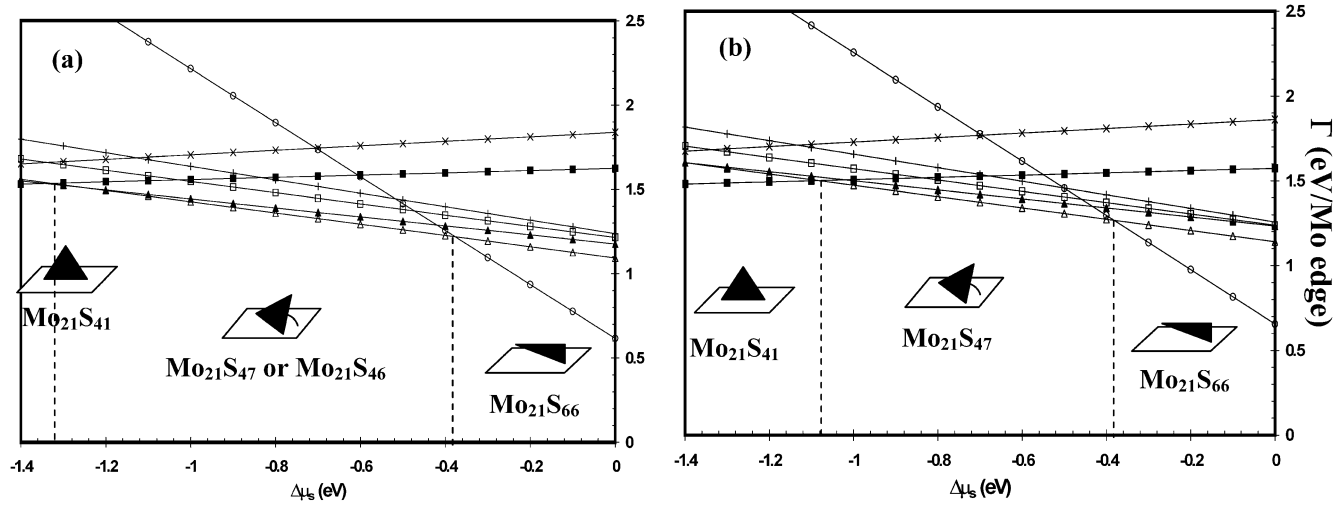

Fig. 14. Gibbs free energy diagrams of the MoS_2 clusters with $k = 6$ Mo per edge adsorbed on the anatase (TiO_2): (a) (101) surface, (b) (001) surface. ○, $Mo_{21}S_{66}$ (100% S, ∥); +, $Mo_{21}S_{48}$ (50% S, ∥); □, $Mo_{21}S_{47}$ (50% S, e, ∥); △, $Mo_{21}S_{47}$ (50% S, c, tilted); ▲, $Mo_{21}S_{46}$ (50% S, c, e, tilted); ■, $Mo_{21}S_{41}$ (50% S, ed, ⊥); ×, $Mo_{21}S_{40}$, (50% S, ed, c, ⊥).

et al. [37,38], revealing large edge-bonded MoS_2 particles on anatase, whereas single-layer MoS_2 particles with basal bonding are predominant on γ-alumina. However, one must be careful with such a qualitative agreement, because the stacking parameter reported in the studies [37,38] is significantly high for some samples, whereas our work deals only with single sheets, as usually found in industrial catalysts [32].

Two remarks can be made about the impact of the weak interactions (van der Waals or H-bonding) on the stability of edge S-vacancies for parallel clusters. On the one hand, according to our model, van der Waals and H-bonding interactions may modify the 100% S-coverage to 50% S-coverage transition. As appears in the diagrams of Figs. 13 and 14, this transition is shifted to smaller chemical potential values than in the case of smaller clusters or compared with previous works [17,19]. This shift is due to the van der Waals and hydrogen interaction of the S-dimers at the edge with the support, which enhances slightly the adhesion energy of the cluster with 100% S versus the 50% S coverage.

On the other hand, the stability of edge S atoms belonging to parallel clusters with 50% S coverage is enhanced slightly by H-bonding. In contrast to γ-alumina, large parallel clusters interact less strongly via hydrogen bonds (M–OH···S) with the anatase support, because of the smaller hydroxylation state of anatase. As a consequence, the creation of edge S-vacancies on large clusters (leading to $Mo_{21}S_{47}$) lying parallel to the support is easier on the dehydroxylated (100) alumina surface and on anatase surfaces than on the hydroxylated (110) alumina surface. To a certain extent, this may

also explain the lower HDS activity of γ-alumina-supported MoS_2 compared with anatase catalysts.

4. Discussion

As mentioned in the Introduction, the higher HDS activity of anatase-supported MoS_2 catalysts has often been referred to in the literature as a manifestation of a direct promotional effect of Ti^{3+} species [10,14,15]. It was shown in [27] that the anatase (001) surface is partially sulfided, explaining the perturbation of the Ti $2p$ level, as observed by XPS [14] and UV–vis spectra [10]. According to thermodynamic considerations similar to those in [27], a pure TiS_2 is not stable versus anatase for realistic partial pressures of H_2S (5 bar) and H_2O (0.01 bar), and at $T = 600$ K, the Gibbs free energy of the reaction $TiO_2 + 2H_2S \rightarrow TiS_2 + 2H_2O$ is strongly positive: +0.74 eV per Ti atom. Furthermore, the energetic balance for a TiMoS mixed phase leads to similar conclusions, assuming that Ti would be transferred from the stable anatase surface to the active MoS_2 (and would be located in the substitution of Mo either at the Mo-edge or at the S-edge, as for the Co or Ni promoter atoms [18]). The most favorable case is described by the following chemical process:

$$\tfrac{3}{4}Mo_4S_9 + TiO_2(101) + \tfrac{9}{4}H_2S \rightarrow TiMo_3S_9 + \tfrac{1}{4}H_2 + 2H_2O, \quad (17)$$

where $TiO_2(101)$ represents the anatase (101) dehydrated surface, Mo_4S_9 is the stable slab exhibiting the Mo- and S-edge, and $TiMo_3S_9$ is the stable slab used for the TiMoS phase, where Ti is located at the S-edge with 50% S.

For the usual $p_{H_2S}/p_{H_2} = 0.05$ and $p_{H_2O} = 0.01$ bar, and at 600 K, the calculated Gibbs free energy (+0.84 eV per Ti atom) does not favor the TiMoS phase. Chemical processes similar to (17), where Ti is located at the Mo-edge, are even less favorable energetically. In contrast, similar thermodynamic calculations comparing the stability of the oxide states of Mo, Co, or Ni with their sulfided forms (MoS_2, Co_9S_8, Ni_3S_2 or CoMoS, NiMoS) favor the latter. Such thermodynamic considerations rule out the proposal of a direct promoting effect of Ti involving the formation of the TiS_2 or TiMoS phases [45].

The results presented above show that the anatase support is able to interact strongly with the Mo-edges or Mo-corners of the clusters and thus stabilizes Mo_6S_{13}, Mo_6S_{11}, and Mo_6S_{10} clusters exhibiting sulfur deficiencies under HDS conditions. On the one hand, the stabilization of Mo_6S_{13}, Mo_6S_{11}, or Mo_6S_{10} clusters through multiple Mo–O–Ti or Mo–S–Ti anchoring (so-called edge-bonded clusters) is induced by the epitaxial relationship (geometric effect) between the surface structure of anatase and the Mo-edge structure. This leads to the formation of four-membered rings, Mo–S(O)–Ti–S(O)–Mo. On the other hand, the stronger Lewis basicity of the Ti–μ_2-O or Ti–μ_2-S species involved in the Mo–O–Ti or Mo–Ti–S bridges implies that the electronic donation from the μ_2-O $2p$ orbitals to the Mo $4d$ orbitals enhances the stabilization of the Mo_6S_{13} cluster versus Mo_6S_{14}. Using the language of homogeneous catalysis, we suggest that these two coupled effects (geometric and electronic) induce a so-called strong chemical ligand effect of the anatase support acting on the MoS_2 active phase. For anatase, this effect stabilizes more S-deficient Mo_6S_n clusters. To some extent, this behavior is analogous to the interpretation of the strong metal-support interaction (SMSI) effect proposed by Tauster et al. [46], who reported a strong decrease in the H_2 and CO chemisorption for supported metal catalysts exhibiting SMSI. In our case, the stronger "chemical ligand effect" of anatase induces a decrease in the S-species stability on the active phase. In contrast, the surface μ_3-O- and Al-species of the γ-Al_2O_3 (100) surface are not favorable for multiple Mo–O–Al bridges. The high hydroxylation state of the (110) surface of γ-Al_2O_3 enhances slightly the multiple anchoring of the active phase (even on γ-alumina) from a geometrical point of view. However, the impact remains weak, and no significant ligand effect of the γ-alumina (110) or (100) surfaces is revealed.

The concept of the ligand effect can be extended to the gas phase itself. Under strong sulfiding conditions ($\Delta\mu_S > -0.2$ eV), our simulations show that the fully sulfided Mo_6S_{24} cluster is stable. The interaction with the support is prevented by the high sulfidation state of the active phase: only weak electrostatic interactions or eventually H-bonds occur between the S atoms of the basal plane and the support. This means that for such a high $\Delta\mu_S$, the support's "chemical ligand effect" vanishes and is replaced by a weak ligand effect governed by van der Waals interactions and/or H-bonds. Because of the intrinsic physical nature of these weak interactions, we define it as a "physical ligand effect" of the support. At the same time, for high $\Delta\mu_S$, the chemical state of the active phase is determined by the S-species present in the gas phase and adsorbing strongly on the active phase. Because such gas-phase S-species modify the chemical behavior of the active phase, we deduce that we are in reaction conditions where the "chemical ligand effect" is controlled by the gas phase.

When considering size effects, we have found that van der Waals and H-bond contributions (the latter play a role only for highly hydrated surfaces such as the alumina (110) surface) reduce the stability of perpendicular or tilted MoS_2 clusters. The stronger "chemical ligand effect" of the anatase support makes possible the thermodynamic stabilization of clusters with a Mo-edge length smaller than 45 Å (on the (001) surface) in perpendicular or tilted orientations. For γ-alumina, most MoS_2 particles with an edge length larger than 10 Å should lie in a parallel configuration on the support. As a consequence, being given the HDS conditions and the particle size, anatase exhibits more S-deficient particles than γ-alumina.

For MoS_2 particle sizes beyond these size limits, the chemical ligand effect of the support vanishes, whereas

the "physical ligand effect" governed by hydrogen bonds (OH···S) and van der Waals interaction becomes predominant. When the OH group concentration is rather high, as on the (110) surface of γ-alumina, OH···S interactions stabilize less sulfur-deficient clusters lying in a parallel orientation.

All of these different new insights may bring arguments in line with the lower HDS activity of γ-alumina-supported MoS_2 versus anatase-supported MoS_2.

5. Conclusions

We have shown how the supported catalyst's active phase is influenced under reaction conditions by competing "ligand effects" induced by both the gas phase and the support. For very high partial pressures of H_2S, the "chemical ligand effect" of S-species present in the gas phase is predominant. For HDS conditions, the "chemical ligand effect" depends on the size of the active phase particles.

MoS_2 particles with an edge length smaller than 10 Å (i.e., a diameter of $\sim$20 Å for hexagonal particles) on γ-alumina and smaller than 45 Å (i.e., a diameter of $\sim$90 Å) on anatase interact more strongly with the support, acting as a "ligand" modifying the chemical properties of the Mo_6S_n clusters. In the case of anatase (TiO_2), the "chemical ligand effect" on the Mo_6S_n clusters strengthened by the epitaxial relationship permits the creation of more sulfur-deficient edge-bonded particles in tilted or perpendicular orientations. This might explain the enhancement of the observed HDS activity of anatase-supported MoS_2 catalysts. For MoS_2 particles with an edge length larger than 10 Å (respectively 45 Å) on γ-alumina (respectively anatase), the support's "chemical ligand effect" vanishes and is replaced by a "physical ligand effect" driven by van der Waals forces or H-bonds, which stabilizes parallel adsorption of the MoS_2 sheet. To a certain extent, this "physical ligand effect" stabilizing S atoms on the active phase favors less sulfur-deficient particles.

The positive "chemical ligand effect" of anatase is proposed as an interpretation of the higher HDS activity observed for anatase-supported MoS_2 active phase versus γ-alumina-supported MoS_2.

We plan to generalize this concept to the so-called S-edge orientation of the MoS_2 active phase, and beyond to clusters representing the Co(Ni)MoS-promoted active phase.

Acknowledgments

This work has been undertaken within the Groupement de Recherche Européen "Dynamique Moléculaire Quantique Appliquée à la Catalyse," a joint project of IFP-CNRS-TOTAL-Universität Wien. The authors are grateful to Prof. Steve C. Parker from the University of Bath for a careful reading of the paper.

References

[1] H. Topsøe, B.S. Clausen, F.E. Massoth, in: J.R. Anderson, M. Boudart (Eds.), Hydrotreating Catalysis–Science and Technology, vol. 11, Springer, Berlin/Heidelberg, 1996.

[2] R. Prins, in: G. Ertl, H. Knözinger, J. Weitkamp (Eds.), Handbook of Heterogeneous Catalysis, vol. 4, Wiley–VCH, Weinheim, 1997, p. 1908.

[3] P. Euzen, P. Raybaud, X. Krokidis, H. Toulhoat, J.-L. Le Loarer, J.-P. Jolivet, C. Froidefond, in: F. Schüth, K.S.W. Sing, J. Weitkamp (Eds.), Handbook of Porous Solids, vol. 3, Wiley–VCH, Weinheim, 2002, p. 1591.

[4] S. Dzwigaj, C. Louis, M. Breysse, M. Cattenot, V. Bellière, C. Geantet, M. Vrinat, P. Blanchard, E. Payen, S. Inoue, H. Kudo, Y. Yoshimura, Appl. Catal. B: Environ. 41 (2003) 181.

[5] B.S. Clausen, H. Topsøe, R. Candia, J. Villadsen, B. Lengeler, J. Als-Nielsen, F. Christensen, J. Phys. Chem. 85 (1981) 3868.

[6] R.G. Leliveld, A.J. van Dillen, J.W. Geus, D.C. Koningsberger, J. Catal. 165 (1997) 184.

[7] H. Shimada, Catal. Today 86 (2003) 17.

[8] M. Cornac, A. Janin, J.C. Lavalley, Infrared Phys. 24 (1984) 143.

[9] N.-Y. Topsøe, H. Topsøe, J. Catal. 139 (1993) 641.

[10] J. Ramirez, L. Cedeno, G. Busca, J. Catal. 184 (1999) 59.

[11] J. Ramirez, S. Fuentes, G. Díaz, M. Vrinat, M. Breysse, M. Lacroix, Appl. Catal. 52 (1989) 211.

[12] M. Breysse, J.L. Portefaix, M. Vrinat, Catal. Today 10 (1991) 489.

[13] M. Breysse, P. Afanasiev, C. Geantet, M. Vrinat, Catal. Today 86 (2003) 5.

[14] L. Coulier, J.A.R. van Veen, J.W. Niemantsverdriet, Catal. Lett. 79 (2002) 149.

[15] D. Wang, W. Qian, A. Ishihara, T. Kabe, Appl. Catal. A: Gen. 224 (2002) 191.

[16] L.S. Byskov, J.K. Nørskov, B.S. Clausen, H. Topsøe, J. Catal. 187 (1999) 109.

[17] P. Raybaud, J. Hafner, G. Kresse, S. Kasztelan, H. Toulhoat, J. Catal. 189 (2000) 129.

[18] P. Raybaud, J. Hafner, G. Kresse, S. Kasztelan, H. Toulhoat, J. Catal. 190 (2000) 128.

[19] H. Schweiger, P. Raybaud, G. Kresse, H. Toulhoat, J. Catal. 207 (2002) 76.

[20] H. Schweiger, P. Raybaud, H. Toulhoat, J. Catal. 212 (2002) 33.

[21] S. Cristol, J.-F. Paul, E. Payen, D. Bougeard, S. Clémendot, F. Hutschka, J. Phys. Chem. B 106 (2002) 5659.

[22] M.V. Bollinger, K.W. Jacobsen, J.K. Nørskov, Phys. Rev. B 67 (2003) 085410.

[23] X. Krokidis, P. Raybaud, A.-E. Gobichon, B. Rebours, P. Euzen, H. Toulhoat, J. Phys. Chem. B 105 (2001) 5121.

[24] M. Digne, P. Sautet, P. Raybaud, P. Euzen, H. Toulhoat, J. Catal. 211 (2002) 1.

[25] M. Digne, P. Sautet, P. Raybaud, P. Euzen, H. Toulhoat, J. Catal. 226 (2004) 54.

[26] C. Arrouvel, M. Digne, M. Breysse, H. Toulhoat, P. Raybaud, J. Catal. 222 (2004) 152.

[27] C. Arrouvel, M. Breysse, H. Toulhoat, P. Raybaud, J. Catal. 226 (2004) 260.

[28] P. Faye, E. Payen, A. Datta, J. Catal. 179 (1998) 560.
[29] A. Ionescu, A. Allouche, J.-P. Aycard, M. Rajzmann, R. Le Gall, J. Phys. Chem. B 107 (2003) 8490.
[30] B. Hinnemann, J.K. Norskov, H. Topsøe, J. Phys. Chem. B 109 (2005) 2245.
[31] C. Wolverton, K.C. Haas, Phys. Rev. B 63 (2001) 024102.
[32] M. Perez De la Rosa, S. Texier, G. Berhault, A. Camacho, M.J. Yacaman, A. Mehta, S. Fuentes, J.A. Montoya, J. Catal. 225 (2004) 288.
[33] J.P. Perdew, Y. Wang, Phys. Rev. B 45 (1992) 13244.
[34] G. Kresse, J. Furthmüller, Comput. Mater. Sci. 6 (1996) 15.
[35] G. Kresse, D. Joubert, Phys. Rev. B 59 (1999) 1758.
[36] M.V. Bollinger, K.W. Jacobsen, J.K. Nørskov, J.V. Lauritsen, S. Helveg, F. Besenbacher, Phys. Rev. Lett. 87 (2001) 6803.
[37] Y. Sakashita, Y. Araki, H. Shimada, Appl. Catal. A 215 (2001) 101.
[38] Y. Sakashita, Y. Araki, K. Honna, H. Shimada, Appl. Catal. A 197 (2000) 247.
[39] E. Payen, S. Kasztelan, S. Houssenbay, R. Szymansky, J. Grimblot, J. Phys. Chem. 93 (1989) 6501.
[40] L. Benco, J. Hafner, F. Hutschka, H. Toulhoat, J. Phys. Chem. B 107 (2003) 9756.
[41] H. Rydberg, M. Dion, N. Jacobson, E. Schröder, P. Hyldgaard, S.I. Simak, D.C. Langreth, B.I. Lundqvist, Phys. Rev. Lett. 91 (2003) 126402.
[42] A.K. Rappe, C.J. Casewit, K.S. Colwell, W.A. Goddard III, W.M. Skiff, J. Am. Chem. Soc. 114 (1992) 10024.
[43] J. Sun, J. Phys. Chem. B 102 (1998) 7338.
[44] Accelrys; Compass and UFF are distributed within the Cerius^2 and Materials Studio package by Accelrys (http://www.accelrys.com) ed.
[45] D. Wang, X. Li, E.W. Qian, A. Ishihara, T. Kabe, Appl. Catal. A: Gen. 238 (2003) 109.
[46] S.J. Tauster, S.C. Fung, R.L. Garten, J. Am. Chem. Soc. 100 (1978) 170.